Contents lists available at ScienceDirect

Arabian Journal of Chemistry

journal homepage: www.ksu.edu.sa

Interaction mechanism of nordentatin with human α-1 acid glycoprotein and human colorectal cancer HCT-116 cells

Bo Yi [a,1], Li Zhang [b,1], Haiyang Zhou [a,*]

[a] Department of Colorectal Surgery, Sichuan Clinical Research Center for Cancer, Sichuan Cancer Hospital, & Institute, Sichuan Cancer Center, Affiliated Cancer Hospital of University of Electronic Science and Technology of China, Chengdu 610041, China
[b] Department of Medical Oncology, Sichuan Clinical Research Center for Cancer, Sichuan Cancer Hospital, & Institute, Sichuan Cancer Center, Affiliated Cancer Hospital of University of Electronic Science and Technology of China, Chengdu 610041, China

ARTICLE INFO

Keywords:
Nordentatin
α-1 acid glycoprotein
Colorectal cancer
Mechanism

ABSTRACT

Plasma protein binding of therapeutic bioactive materials, especially anticancer compounds can play an important role in their pharmacokinetics and pharmacodynamics. Human α-1 acid glycoprotein (AGP) has shown potential binding affinities to different endogenous and exogenous ligands due to its unique binding site composed of eight anti-parallel β-sheets. Therefore, in this study, the interaction of nordentatin, a member of coumarins with a chemical formula of $C_{19}H_{20}O_4$ with AGP, was measured by multi-spectroscopic and theoretical approaches. Afterward, the anticancer potency of nordentatin against human colorectal cancer HCT-116 cells was assessed. The fluorescence quenching of AGP was observed upon binding of nordentatin through a static quenching mechanism. The spontaneous hydrophobic interaction of nordentatin with AGP had a binding constant value (K_b) of 10^4 M^{-1} with a marginal change in the secondary structure of AGP. Cellular assays demonstrated that nordentatin exhibited promising inhibitory effects on the cellular growth of HCT-116 cells through increasing the levels of intracellular ROS and [Ca^{2+}], while it remarkably triggered the MMP reduction. Also, RT-qPCR analysis disclosed that nordentatin stimulated apoptosis by overexpression of P53, Bax/Bcl-2, cytochrome *c*, caspase-9, and caspase-3 mRNA. Overall, these findings suggested that nordentatin, in addition to potential binding to plasma protein, could be used as an effective preventive or curative plant-based therapy for colorectal cancer.

1. Introduction

Human α-1 acid glycoprotein (AGP, orosomucoid, acute phase protein in plasma, with a concentration of 0.4–1.1 mg/mL) is known as a highly glycosylated protein (45 %) with a molecular weight of 37–54 kDa and a low pI of 2.8–3.8 (Luo, Lei et al., 2015). AGP has shown a wide range of activities such as a disorder marker, modulating immunity and regulating the sphingolipid metabolism (Luo, Lei et al., 2015). Additionally, it has been widely demonstrated that AGP has a potential binding capability to several endogenous and exogenous ligands mediated by eight anti-parallel β-sheets (Zsila and Mády, 2008, Luo, Lei et al., 2015, Bteich, 2019, Schmidt, Zehe et al., 2023). Plasma protein binding of drugs can play a significant role in their pharmacokinetics and pharmacodynamics (Schmidt, Gonzalez et al., 2010). As a result, the research on the interaction characteristics of ligands/drugs with AGP has received a great deal of attention (Jiang, Hu et al., 2023, Kou, Li et al., 2023).

Nordentatin, a member of coumarins [a pyranocoumarin with a chemical formula of $C_{19}H_{20}O_4$, 5-hydroxy-2,2-dimethyl-6-(2-methylbut-3-en-2-yl)pyrano[2,3-h]chromen-8-one] is presented in *Enkleia* (Luo, Boonyaratanakornkit et al., 1986) and *Clausena* (Luo, Boonyaratanakornkit et al., 1986) plants. Nordentatin has depicted different pharmacological activities, including neuritogenic (Jantakoon, Tadtong et al., 2012), antioxidant (Jantakoon, Tadtong et al., 2012) and anticancer (Boonyarat, Boonput et al., 2022). Regarding the anticancer activities of nordentatin, it has been reported that its derivatives can trigger anticancer activities mediated by the regulation of cAMP (Abdjan, Aminah et al., 2020) and GSK-3 (Boonyarat, Boonput et al., 2022)

Peer review under responsibility of King Saud University.

* Corresponding author at: 55 Section 4, Renmin South Road, Chengdu City, Sichuan Province, China.
E-mail address: Haiyangzhou23@outlook.com (H. Zhou).

[1] Contribute equally to this study.

https://doi.org/10.1016/j.arabjc.2023.105432
Received 15 September 2023; Accepted 1 November 2023
Available online 2 November 2023

signaling pathways. However, there has not been much research done on the other possible anticancer mechanisms stimulated by nordentatin.

As colorectal cancer (CRC), the third most widespread cancer globally had serious impacts on medical care and the global economy, the utilization of different bioactive compounds for CRC treatment has received remarkable interest in recent years (Gavrilas, Cruceriu et al., 2022, Hossain, Karuniawati et al., 2022). Natural plant-based metabolites may provide us with promising anticancer alternatives, because of their effective chemopreventive or chemotherapeutic features (Siddiqui, Jahan et al., 2022, Ullah, Rehman et al., 2022).

Based on these facts, in this paper, the interaction of nordentatin with AGP was explored by different spectroscopy techniques combined with a molecular docking study to reveal the binding characteristics of this potential bioactive compound. Then, the anticancer effect of nordentatin on human colorectal cancer HCT-116 and the associated apoptosis mechanism were explored by different cellular and molecular assays.

2. Materials and methods

2.1. Materials

Nordentatin ≥(95 % LC/MS-ELSD, CAS Number: 17820–07-4), human α-1 acid glycoprotein (≥99 % agarose gel electrophoresis, CAS Number: 66455–27-4), Dulbecco's Modified Eagle Medium (DMEM), fetal bovine serum (FBS), and methylthiazolyldiphenyl-tetrazolium bromide (MTT) were purchased from Sigma-Aldrich (Shanghai, China). All other reagents were of analytical grade.

2.2. Preparation of solutions

10 mM sodium phosphate buffer (pH 7.4) was used throughout the nordentatin-AGP interaction study and AGP was used without further purification. Stock solution (2 mg/ml) of AGP was prepared in sodium phosphate buffer (10 mM, pH 7.4) and its concentration was calculated spectroscopically using $\varepsilon_{280\ nm} = 8.93$ (Abdelhameed, Ajmal et al., 2016). Nordentatin was dissolved in absolute alcohol and during protein assays, nordentatin volume was below 2 % of the total volume.

2.3. UV–visible study

A JASCO V-530 UV–visible spectrophotometer was used to study the absorption properties of free AGP and AGP-nordentatin complex. 10 μM of AGP was added by increasing concentrations of nordentatin to reach the molar ratio of nordentatin: AAG = 10:1. The linear double reciprocal plot of $1/A\text{-}A_o$ against 1/molar nordentatin concentration was plotted and binding constant (K_b) value was then calculated by the ratio of intercept to the slope (Abdelhameed, Ajmal et al., 2016). A_o and A define the free AGP and AGP-nordentatin absorbance at 280 nm. All studies were performed at room temperature and the AGP samples were corrected against nordentatin absorbance.

2.4. Fluorescence quenching study

All fluorescence studies were performed on a Hitachi F-7000 fluorescence spectrophotometer (5 J1-004) combined with a water circulator. Spectra measurements were carried out in the wavelength range of 310–450 nm with an excitation and emission slit width of 5 nm and 10 nm, respectively, while AGP samples were excited at 280 nm. Titration of 1.5 μM AGP was done at different temperatures of 298 K and in the presence of varying concentrations of nordentatin to achieve nordentatin:AGP molar ratios from 1:1 to = 10:1. The fluorescence data were corrected against the inner filter effect.

2.5. Synchronous fluorescence spectroscopy

Synchronous fluorescence spectroscopy measurements of AGP in the presence and absence of nordentatin were carried out by fixing the scanning interval of $\Delta\lambda$ ($\lambda_{em} - \lambda_{ex}$) at 15 and 60 nm to check the change in the micro-environment around Tyr and Trp residues, respectively. All other parameters for synchronous fluorescence spectroscopy were fixed similar to the fluorescence quenching study.

2.6. Molecular docking

The crystal structure of AGP was downloaded from Brookhaven Protein Data Bank with PDB ID:3KQ0. The coordinate 3D sdf file of nordentatin (CID 5320206) was obtained from Pub Chem. Molecular docking simulations were performed using Vina AutoDock software. Grid size was set at 39, 37 and 42 along the X, Y and Z axes. A rigid structure was set for AGP chains, while nordentatin was allowed to be flexible and have possible rotation and conformation. Spacing, mode numbering, energy range and exhaustiveness were set as defaults. The lowest binding energy out of 20 docking results was selected for further analyses.

2.7. Far-UV circular dichroism (CD) measurement

Far-UV CD spectra of AGP (5 μM) in the absence and presence of different concentrations of nordentatin (nordentatin:AGP molar ratios from 1:1 to = 10:1) were done using a JASCO-J815 spectropolarimeter at room temperature. The scan speed of spectra was set at 50 nm/min along with a response time of 2 s. CD spectra were read in the wavelength range of 200–260 nm using a quartz cuvette of 1 mm path length. Data was analyzed using CDNN software. All data were corrected against nordentatin CD signal.

2.8. Cell culture

The HCT-116 cell line was purchased from the American Type Culture Collection (ATCC). HCT-116 cells were grown in DMEM supplemented with 10 % (v/v) FBS, 1 % nonessential amino acid, 100 U/mL penicillin/streptomycin, and 2.2 g/L $NaHCO_3$ in CO_2 incubator at 37 °C.

2.9. MTT assay

Cell viability was assessed by an MTT assay as reported previously (Yu, Wang et al., 2022). In brief, the cells were seeded in 96-well plates (1×10^4 cells/well) for 24 h. After removing the cell culture medium, the cells were incubated with the fresh medium containing different concentrations of nordentatin (1–200 μM) for 48 h. After medium removal and washing, 100 μL MTT solution (5 mg/mL) was added to each well and incubated at 37 °C for another 4 h followed by supernatant removal and the addition of 100 μL DMSO. The optical density was read at 490 nm on a microplate reader (Bio Rad Laboratories, Hercules, CA, USA). The cells without any nordentatin inhibition were regarded as a negative control.

2.10. Mitochondrial membrane potential (MMP), intracellular ROS and $[Ca^{2+}]$ assays

The cells were seeded into 6-well plates (1×10^5 cells/well) for 24 h and then exposed to the complete medium and nordentatin (IC_{50}: 75 μg/mL) for 48 h. Then the analyses of MMP, intracellular ROS and $[Ca^{2+}]$ were done as previously reported (Yu, Wang et al., 2022).

2.11. Reverse transcription quantitative real-time PCR assay (RT-qPCR)

The cells were inoculated at 6-well plates (1×10^5 cells/well) for 24 h, and then incubated with the complete medium and nordentatin (IC_{50}:

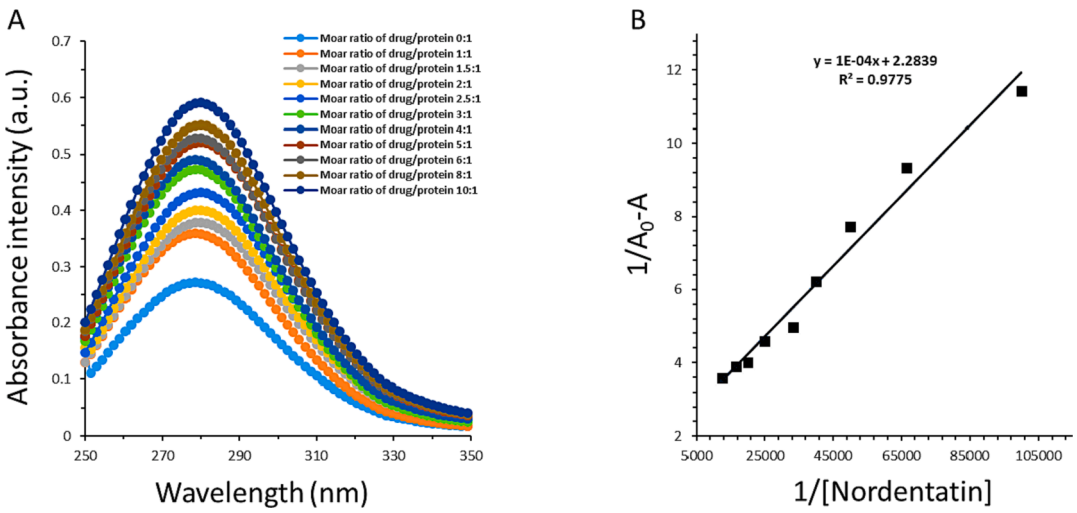

Fig. 1. (A) UV–visible measurement of AGP following the interaction with nordentatin at different molar ratios of nordentatin:AGP at room temperature. (B) The linear double reciprocal plot of $1/A\text{-}A_o$ *vs.* 1/[nordentatin].

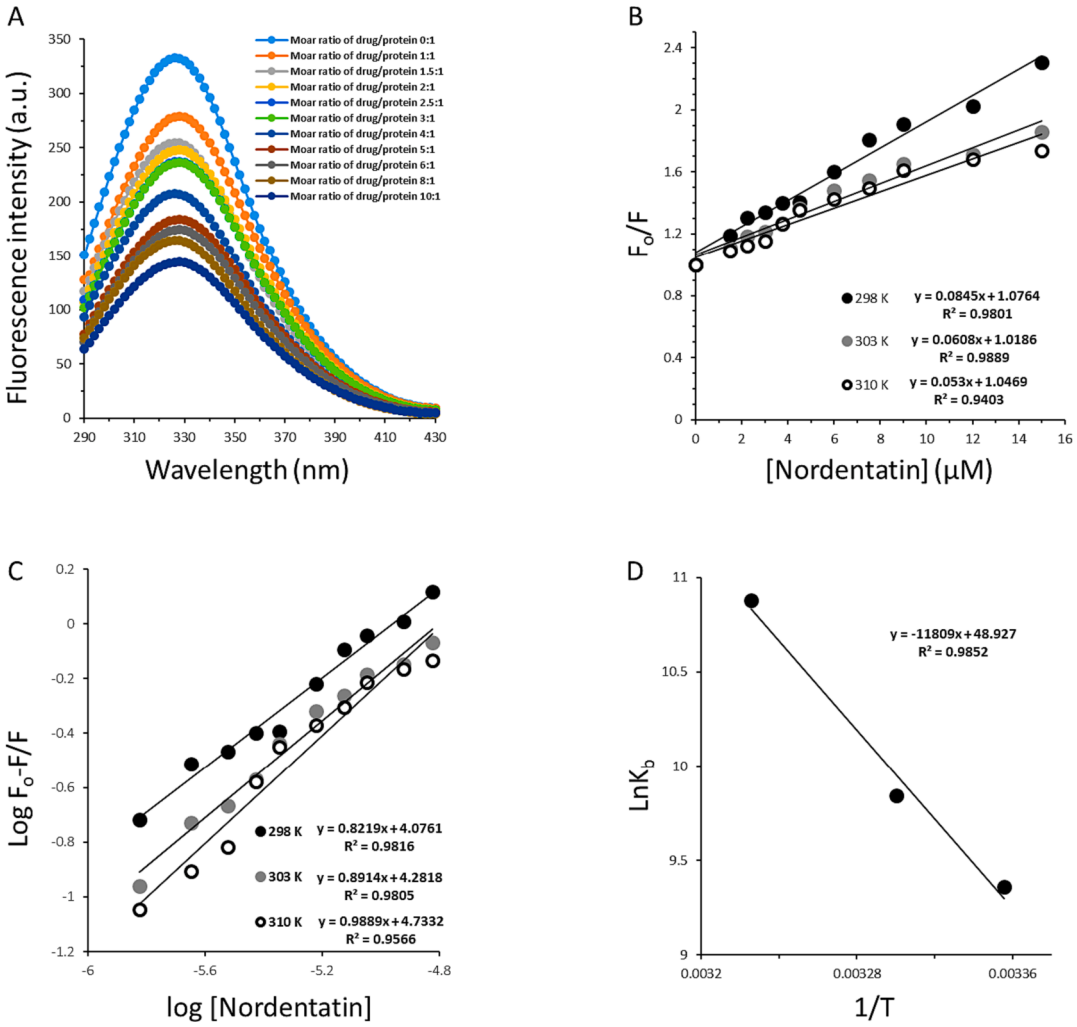

Fig. 2. (A) Steady-state fluorescence measurement of AGP following the interaction with nordentatin at different molar ratios of nordentatin:AGP at room temperature. (B) The linear Stern-Volmer plots for nordentatin:AGP complexes at three different temperatures. (C) The linear modified Stern-Volmer plots for nordentatin:AGP complexes at three different temperatures. (D) The linear Van't hoff plot for nordentatin:AGP complexes.

75 μg/mL) for 48 h. The reverse transcription quantitative real-time PCR (RT-qPCR) assay was then done based on the classical method. Briefly, total RNA was extracted using the RNAprep pure cell kit (TIANGEN, Beijing, China), then reverse transcription and the synthesis of complementary DNA (cDNA) was performed using the rimeScipt RT Reagent Kit (TaKaRa, Kusatsu, Shiga, Japan). The amplification of the cDNA using the BioRad® SYBR qPCR SuperMix and BioRad Real-Time PCR system (USA) was carried out. The relative expression of the target genes was estimated using the classic $2^{-\Delta\Delta Ct}$ method, while β-actin was selected as the housekeeping gene. The primers for p53, Bax, Bcl-2, cytochrome *c*, caspase-9, and caspase-3 were designed with the sequences reported in previous studies (Tsai, Li et al., 2017, Yu, Wang et al., 2022).

2.12. Statistical analyses

The cell-related values were reported as the means ± (SD) from three experiments. SPSS tests were used to analyze significant differences ($p < 0.05$).

3. Results and discussion

3.1. UV–visible study of AGP interaction with nordentatin

UV–Vis absorption spectroscopy as a sensitive technique has been widely used to measure the steady-state interactions of AGP with different ligands (Ajmal, Nusrat et al., 2017, Kou, Li et al., 2023). For AGP, the aromatic amino acids serve as the intrinsic chromophores-inducing characteristics of electronic absorption capacities in the wavelength range of 260–290 nm. Tryptophan (Trp) and Tyr (Tyr) residues in the AGP chain typically depict a UV-absorbance peak around 280 nm (Abdelhameed, Ajmal et al., 2016). Fig. 1A displays that the AGP absorption maximum of 280 nm is mostly derived from aromatic residues. The absorption peak intensity of APG was observed to increase following the addition of nordentatin, suggesting conformational changes in the vicinity of aromatic residues of AGP (Abdelhameed, Ajmal et al., 2016). Indeed, this increase in UV absorbance of AGP upon the addition of nordentatin is based on the presence of more unfolded conformation relative to free AGP (Ajmal, Nusrat et al., 2017).

Also, the increase in the UV–visible absorption spectra of AGP-nordentatin relative to free AGP confirmed the formation of a ground-state AGP-nordentatin complex as reported for AGP and anticancer drug nintedanib in an earlier study (Abdelhameed, Ajmal et al., 2016).

The binding constant (K_b) value was then calculated by the ratio of intercept to slope derived from the linear double reciprocal plot of $1/A\text{-}A_o$ *vs.* 1/[nordentatin] calculated (Fig. 1B). It was deduced that the K_b value for the interaction of AGP with nordentatin was around 2.28×10^4 M^{-1}.

3.2. Fluorescence quenching study of AGP interaction with nordentatin

3.2.1. Quenching mechanism determination

Trp/Tyr quenching was performed to determine the quenching mechanism (static or dynamic) of AGP following the addition of nordentatin with different molar ratios of nordentatin:AGP ranging from 1:1 to 10:1. AGP displayed a significant fluorescence peak around 328 nm following excitation at 280 nm (Fig. 2A). However, the emission intensity of AGP was quenched upon adding nordentatin to AGP, indicating the possible interaction between nordentatin and AGP (Fig. 2A). The values of the fluorescence intensity at 228 nm were used to determine the quenching mechanism and other interaction parameters.

Stern-Volmer equation (Eq. (1)) was used to determine the quenching parameters as follows (Wang, Kou et al., 2020):

$$F_0/F = K_{SV}[Q] + 1 = k_q\tau_0[Q] + 1 \quad (1)$$

Where, F_0 and F are fluorescence intensities of proteins in the absence and presence of quenchers, respectively, K_{SV} is the Stern–Volmer constant, k_q is the bimolecular rate constant, τ_0 is the average fluorescence lifetime of fluorophore ($\sim 10^{-9}$ s), and Q is the concentration of quencher (Abdelhameed, Ajmal et al., 2016). Stern-Volmert plots display a linear relationship between the molar concentration of nordentatin and the values of the F_0/F ratio (Fig. 2B).

The K_{SV} and kq values are then computed and summarized in Table 1.

It was found that kq values at 298 K, 303 K and 310 K are 8.45 ××10^{13} M^{-1} s^{-1}, 6.08 × 10^{13} M^{-1} s^{-1} and 5.30 × 10^{13} M^{-1} s^{-1}, respectively (Table 1), which are greater than the maximum scatter collision quenching constant (2×10^{10} mol^{-1} S^{-1}) (Abdelhameed, Ajmal et al., 2016), suggesting the formation of a ground state complex between AGP and nordentatin (Jiang, Li et al., 2023, Kou, Li et al., 2023). This data is in good agreement with the UV–visible study which stated that a static quenching mechanism occurs following the interaction of AGP with nordentatin (Fig. 1A).

Table 1
The K_{SV} and kq values for the interaction of nordentatin and AGP.

Temperature (K)	K_{sv} ($\times 10^4$ M^{-1})	K_q ($\times 10^{13}$ M^{-1} s^{-1})	R2
298	8.45	8.45	0.9801
303	6.08	6.08	0.9889
310	5.30	5.30	0.9403

Table 2
The binding parameters for the interaction of nordentatin and AGP.

Temperature (K)	$logK_b$	n	R2
298	4.07	0.82	0.9801
303	4.28	0.89	0.9889
310	4.73	0.98	0.9403

3.2.2. Binding parameter determination

When ligands interact/bind independently to a set of binding sites on a biomacromolecule, the equilibrium between interacted and free ligands could be analyzed by a modified Stern–Volmer equation (Eq. (2)) as follows:

$$F_0 - F/F = logK_b + nlog[Q] \quad (2)$$

where n and K_b are the number of binding sites, and binding constant, respectively. Based on this equation (Eq. (2)), the plotted results shown in Fig. 2C depicted a good linearity. The binding parameters were then calculated and summarized in Table 2.

The number of nordentatin molecules binding to AGP was computed to be 0.98 at 310 K, suggesting that AGP interacts with nordentatin in a one-to-one ratio at physiological temperature. The $logK_b$ values of nordentatin calculated from the Y-intercept of Fig. 2C were 4.07, 4.28 and 4.73, which reveals a potential binding of nordentatin to AGP. A good correlation could be observed between K_b values calculated by UV–visible spectroscopy and fluorescence spectroscopy measurement since both techniques yielded K_b values of 10^4 M^{-1}.

Interestingly, the K_b of nordentatin with AGP was stronger at physiological terpature (310 K) than 298 K and is in the range of the Federal Drug Administration (FDA) (Yeggoni, Rachamallu et al., 2015). It has been revealed that in most cases, AGP can serve as a vehicle to bind various drugs (Huang, Cooper et al., 2012, Kou, Li et al., 2023). Therefore, in cancer diseases, the AGP can play a key role in transporting the nordentatin molecules. The abundance of AGP levels in the plasma could influence the protein-nordentatin interactions which cause changes in the mode of nordentatin reaction, biodistribution, efficacy, and elimination (Huang, Cooper et al., 2012). Although, the concentration of AGP is much lower than that of albumin in plasma (Huang, Cooper et al., 2012), AGP can still play a key role in the binding properties of nordentatin with significant clinical applications (Johnson and

Table 3
The thermodynamic parameters for the interaction of nordentatin and AGP.

Temperature (K)	ΔH^0 (kJ/mol)	ΔS^0 (kJ/mol K)	ΔG^0 (kJ/mol)
298	98.01	406.03	−22.98
303			−25.01
310			−27.85

Smith 2006). In agreement with our results, Maruyama et al., reported that coumarin 4-hydroxycoumarin had a binding affinity of 6.1 × lo^4 M^{-1} following the interaction with AGP (Maruyama, Otagiri et al., 1990).

3.2.3. Thermodynamic parameter determination

In general, there are four kinds of non-covalent forces when ligand compounds interact with proteins, which are hydrogen bonds, electrostatic, hydrophobic, and van der Waals forces. Typically, thermodynamic parameters are used as the primary proof to confirm the involvement of various forces in the formation of drug-protein complexes. The changes in enthalpy (ΔH^0) and entropy (ΔS^0) at different temperatures were calculated by using Vant Hoff's equation (Eq. (3)) as follows:

$$lnK_b = -\Delta H^0/RT + \Delta S^0/R \quad (3)$$

where, T and R are absolute temperature and universal gas constant, respectively.

Then, the standard free energy (ΔG^0) was calculated according to the following equation (Eq. (4)):

$$\Delta G^{0=}\Delta H^{0-}T\Delta S^0 \quad (4)$$

Thus, the calculated thermodynamic parameters were determined

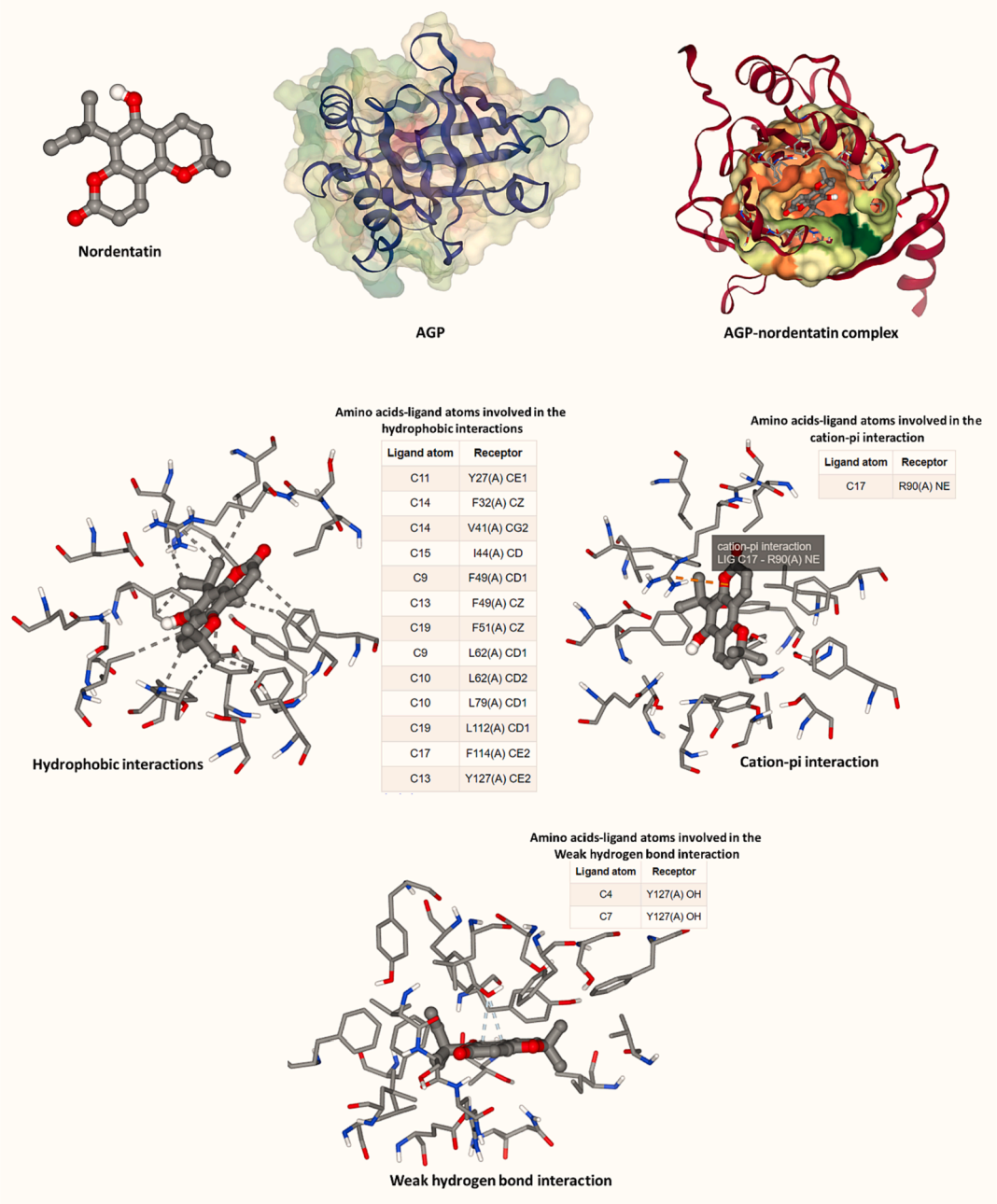

Fig. 3. Molecular docking analysis of nordentatin:AGP complex.

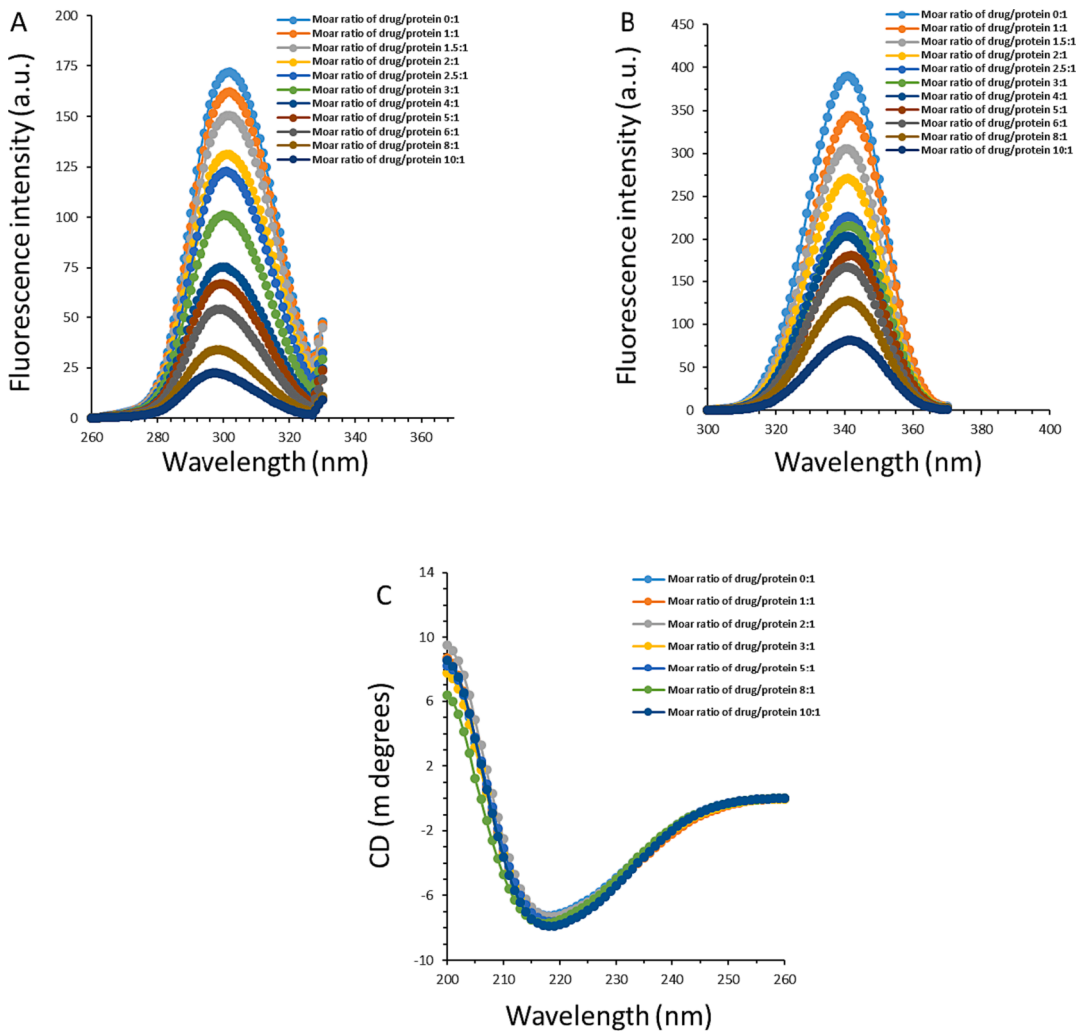

Fig. 4. (A) Synchronous fluorescence measurement of AGP following the interaction with nordentatin at different molar ratios of nordentatin:AGP at room temperature when the Δλ is fixed at 15 nm. (B) Synchronous fluorescence measurement of AGP following the interaction with nordentatin at different molar ratios of nordentatin:AGP at room temperature when the Δλ is fixed at 60 nm. (C) Far-UV CD measurement of AGP following the interaction with nordentatin at different molar ratios of nordentatin:AGP at room temperature.

based on Fig. 2D and the resultant data was listed in Table 3.

The ΔG^0 values were found to be –22.98 kJ/mol K, −25.01 kJ/mol K and −27.85 kJ/mol K at 298 K, 303 K and 310 K, suggesting that the binding interaction of nordentatin with AGP is spontaneous (Jiang, Li et al., 2023). Also, ΔH^0 (98.01 kJ/mol K) *and* ΔS^0 (406.03 kJ/mol K) values for the interaction of nordentatin with AGP signifies the hydrophobic forces mainly contribute to the formation of nordentatin-AGP complex (AlAjmi, Rehman et al., 2020).

3.3. Molecular docking study

Protein–ligand interactions occurring in biological systems can be mimicked by molecular docking analysis. Although the protein functions and binding sites in vitro and in vivo are different from those of *in silico* studies, the molecular interactions underlying protein–ligand interactions can be verified by theoretical analyses (Ajmal, Nusrat et al., 2017, Yeggoni, Meti et al., 2023). Therefore, molecular docking analysis was done to further verify the specific interaction of nordentatin with AGP. The molecular docking simulations were performed to determine the probable nordentatin binding site as well as the energy of nordentatin binding process, upon interaction with AGP. For AGP-nordentatin interaction, binding energy was determined to be to be − 38.07 kJ/mol^{-1}. This amount was greater than the binding energy calculated by fluorescence spectroscopy measurement (–22.98 kJ/mol), suggesting the occurrence of a more complicated interaction between nordentatin and AGP in the experimental solution than that of theoretical analysis. Amino acids contributed to the hydrophobic interaction of AGP and nordentatin were detected to be Tyr27, Phe32, Val41, Ilu44, Phe49, Phe51, Leu62, Leu79, Leu112, Phe144, and Tyr127. However, Arg90 contributes to the formation of cation-pi interaction between AGP and nordentatin. Finally, it was observed that Tyr127 was involved in the formation of weak hydrogen bonds between AGP and nordentatin (Fig. 3).

The molecular docking findings suggested the dominant participation of hydrophobic forces in the interaction process for AGP-nordentatin complexation, followed by weak hydrogen bonds and cation-pi interactions. This data is in good agreement with fluorescence spectroscopy measurements indicated that hydrophobic interactions were the main forces involved in the formation of AGP-nordentatin complex.

Previous reports have also shown that Tyr27 and Tyr127 were presented in the binding pocket of AGP following the interaction with olmutinib ($C_{26}H_{26}N_6O_2S$) (Kou, Li et al., 2023), Janus Kinase inhibitor baricitinib ($C_{16}H_{17}N_7O_2S$) (Jiang, Hu et al., 2023) and antitubercular drug candidates (Zsila, Bősze et al., 2020). It can be then indicated that Tyr residues may play a key role in the interaction of AGP with different

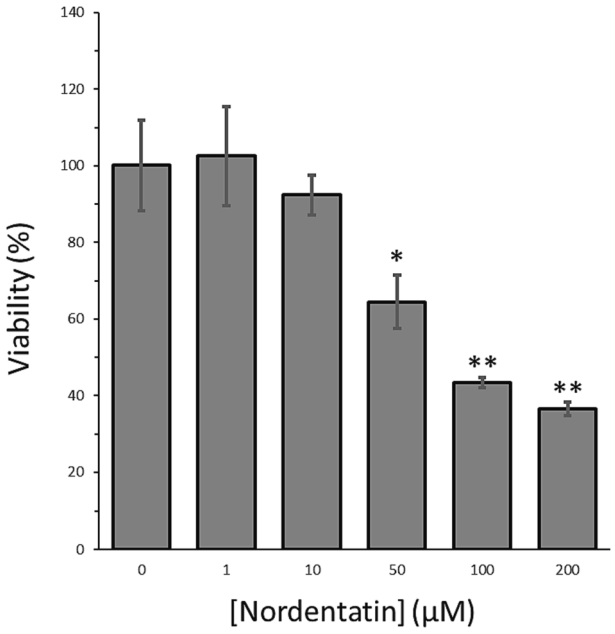

Fig. 5. The MTT assay of HCT-116 cells after interaction with different concentrations of nordentatin after 48 h. The data were shown as means ± SD from three experiments. *P < 0.05, **P < 0.01 relative to control cells.

drugs.

3.4. Structural changes study

Synchronous fluorescence spectroscopy is typically employed to measure the micro-environmental changes in the vicinity of two amino acid residues, Trp and Tyr, following binding ligands (Wang, Sun et al., 2023). This technique provides good selectivity as well as high sensitivity for detecting the conformational changes of proteins (Wang, Kou et al., 2020). When the Δλ is fixed at 15 nm or 60 nm, the changes in the surrounding environment of Tyr or Trp residues can be analyzed, respectively (Jiang, Li et al., 2023, Jiang, Li et al., 2023). As shown in Fig.4A and B, the fluorescence intensity of both Tyr (Fig. 4A) and Trp (Fig. 4B) residues reduced following adding the increasing concentration of nordentatin. Also, the maximum emission wavelength for Tyr residues (Fig. 4A) marginally shifted toward the short wavelength (blue shift) when setting at $\Delta\lambda = 15$ nm while the shift for Trp residues (Fig. 4B) was not almost observed when fixing at $\Delta\lambda = 60$ nm. This data suggested that nordentatin binds closer to Tyr residues relative to Trp residues and the hydrophobicity around Tyr residues increased slightly (Ajmal, Nusrat et al., 2016, Jiang, Li et al., 2023). This data is in good agreement with the molecular docking study, which disclosed that Tyr residues were presented in the binding pocket of AGP upon interaction with nordentatin.(See Fig. 3).

CD measurement is also a sensitive method for characterizing the secondary structure of proteins(Wang, Kou et al., 2020). The CD spectrum in the far UV region (200 to 260 nm) can reflect the secondary structural changes of the protein (Longo, Siligardi et al., 2023, Owczarzy, Rogóż et al., 2023). For AGP secondary structure rich in β-sheet conformation, CD spectrum shows a CD spectrum with one minimum between 215 and 220 nm (Wang, Kou et al., 2020). We discovered

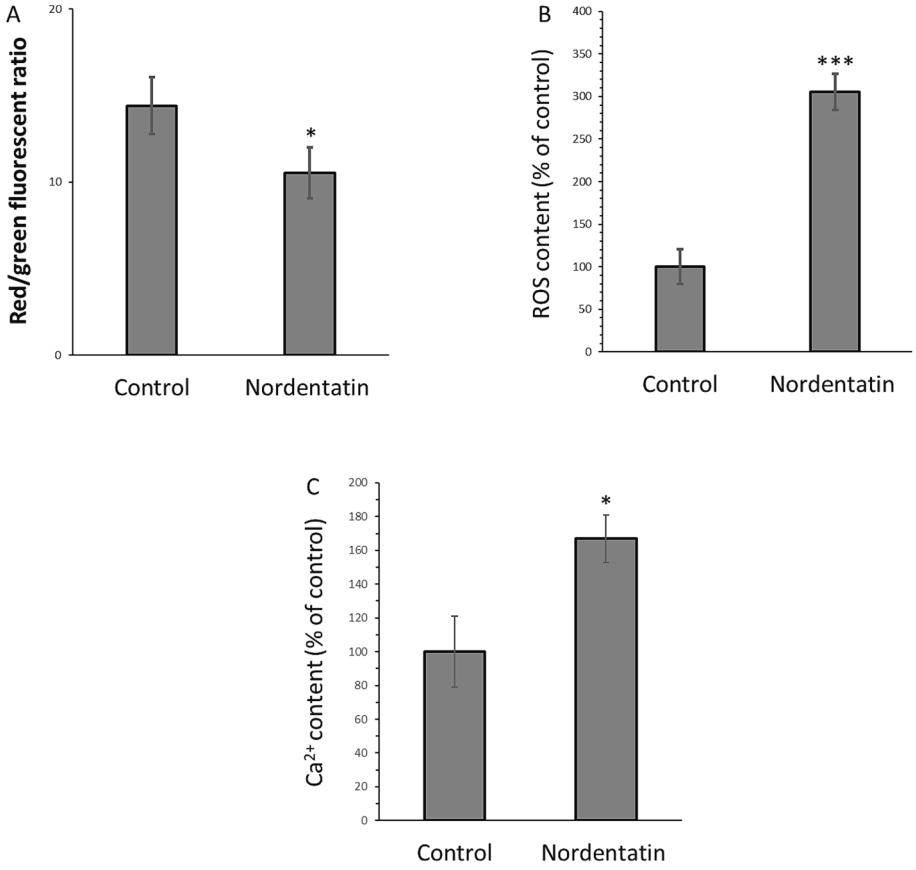

Fig. 6. (A) The measured mitochondrial membrane potential loss, (B) intracellular ROS formation, and (C) intracellular Ca^{2+} of the HCT-116 cells incubated with 75 μM nordentatin for 48 h. *P < 0.05, **P < 0.01, ***P < 0.001 relative to control cells.

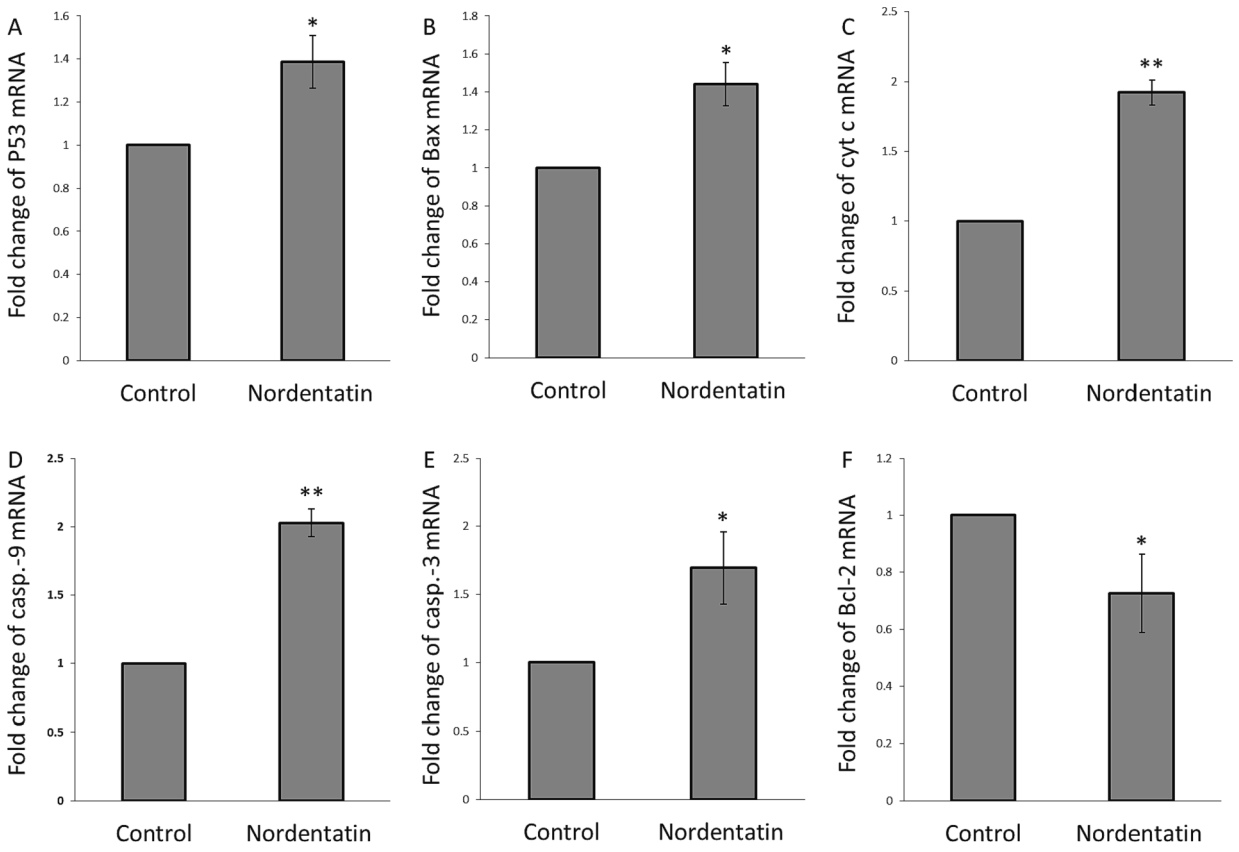

Fig. 7. (A) Fold change of p53 mRNA, (B) fold change of Bax mRNA, (C) fold change of cytochrome *c* mRNA, (D) fold change of caspase-9 mRNA, (E) fold change of caspase-3 mRNA, and (F) fold change of Bcl-2 mRNA in the HCT-116 cells incubated with 75 μM nordentatin for 48 h. *P < 0.05, **P < 0.01, ***P < 0.001 relative to control cells.

earlier using molecular docking and fluorescence spectroscopy that when nordentatin interacts with AGP, new intermolecular interaction forces can form between protein and ligand. These new forces may not only cause some micro-environmental changes in the vicinity of the binding site region, but they may also cause changes in the AGP's secondary structure. As a result, it is crucial to investigate the far-UV CD characteristic of AGP in the presence or absence of nordentatin. As is shown Fig. 4C, a negative CD band around 218 nm was observed for free AGP solution, displaying that the main structure of AGP is composed of β-sheet, which is consistent with studies reported previously (Wang, Kou et al., 2020, Jiang, Hu et al., 2023). However, upon the addition of nordentatin slight changes in the CD spectra of AGP were observed, revealing partial alterations in the secondary structure of AGP following the interaction with nordentatin. Quantification of β-sheet structure in AGP revealed a slight increase in the content of β-sheet structure from 42.97 % for free AGP to 44.39 % for the nordentatin-AGP complex with a nordentatin:AGP molar ratio of 10:1, suggesting partial changes in the secondary structure of AGP occurred following binding to nordentatin.

3.5. Cell viability assay

The cytotoxic effect of nordentatin on HCT-116 cells was assessed at the targeted concentration levels (Fig. 5). Nordentatin at lower concentration levels (1 and 10 μM) displayed no significant cytotoxicity on the cells, resulting in the cell viability values of 102.54–92.37 %; however, nordentatin at higher concentrations (50—200 μM) with 48 h treatment time resulted in efficient cell death with the cell viability values of 64.40–36.53 % (Fig. 5). This fact indicated that nordentatin was very cytotoxic to the cells at concentrations above 10 μM. It was then possible to estimate the IC_{50} value of nordentatin scientifically with an IC_{50} value of 75 μM (48 h). The findings confirmed that nordentatin had an obvious growth inhibition on the HCT-116 cells, suggesting the used coumarin moiety made a significant involvement in the growth inhibition of nordentatin on the cancer cell.

Boonyarat et al., exhibited that nordentatin with a concentration of 100 μM triggered a statistically significant reduction in the percentage of neuroblastoma (SH-SY5Y) cell viability compared to the control group ($p < 0.01$) after 24 h of incubation (Boonyarat, Boonput et al., 2022). Additionally, it was revealed that the IC_{50} concentrations of nordentatin isolated from *C. harmandiana* against the human liver cancer cell line (HepG2), HCT-116 and the human lung adenocarcinoma cell line (SK-LU-1) were 29.9 ± 3.2 μM, 63.6 ± 2.3 μM and 67.3 ± 1.2 μM, respectively, after 24 h (Jantamat, Weerapreeyakul et al., 2019).

3.6. MMP loss and intracellular level of ROS and [Ca^{2+}]

When HCT-116 cells were incubated with 75 μM nordentatin for 48 h, the findings (Fig. 6A) demonstrated that the treated cells had a decreased MMP. The control cells showed a red/green fluorescent ratio of 14.41, while the nordentatin-exposed cells using a concentration level of 75 μM demonstrated a lower ratio of 10.52. This data suggested that nordentatin was capable of damaging the mitochondrial membranes of the HCT-116 cells, leading to MMP loss. It was also expressed that nordentatin led to an increased ROS level in HCT-116 cells (Fig. 6B), indicating the nordentatin sample induced a pro-oxidation status in the cells. In detail, relative to the control cells, the nordentatin-incubated cells using a concentration level of 75 μM had ROS level of 305.54 % (Fig. 6B). Clearly, nordentatin was shown to be active in promoting intracellular ROS generation in the HCT-116 cells.

The nordentatin-incubated HCT-116 cells also had significant intracellular [Ca^{2+}] release, deduced from the enhanced content of intracellular [Ca^{2+}] (Fig. 6C). In comparison with the control HCT-116 cells

(100 % [Ca^{2+}] value), the cells incubated with nordentatin at 75 μM showed [Ca^{2+}] value of 166.85 %. Overall, this data confirmed that nordentatin is able to promote intracellular [Ca^{2+}] release. In general, a high level of intracellular ROS in the cancer cells may trigger endoplasmic reticulum (ER) stress; afterwards, ER stress results in the release of abundant intracellular [Ca^{2+}] into the cytoplasm, which [Ca^{2+}] overload ultimately leads to MMP loss (Kim, Cho et al., 2013, Yu, Wang et al., 2022, Zhou, Jing et al., 2022). Therefore, the interplay of ROS, intracellular [Ca^{2+}] and mitochondrial homeostasis can be responsible for inhibition of HCT-116 cancer cell proliferation induced by nordentatin.

Furthermore, based on these outcomes (Fig. 6), it can be possible that nordentatin might trigger its anticancer activities to HCT-116 cells via exerting cell apoptosis. To further verify this hypothesis, RT-qPCR analysis was done.

3.7. Expression levels of the apoptosis-related genes

When the HCT-116 cells were exposed to nordentatin, the mRNA expression of 6 apoptosis-associated genes was assessed (Fig. 7). The control samples were defined with a relative gene expression level of 1.0-fold for all genes.

Overall, nordentatin was shown to upregulate the expression levels of the 5 pro-apoptotic genes, P53 (Fig. 7A), Bax (Fig. 7B), cytochrome *c* (Fig. 7C), caspase-9 (Fig. 7D), and caspase-3 (Fig. 7E), however, downregulate the expression level of an anti-apoptotic gene, Bcl-2 (Fig. 7F). This data revealed that the nordentatin had a great apoptosis induction in the HCT-116 cells.

Therefore, it can be suggested that nordentatin stimulates apoptosis mainly associated with a p53-dependent cell signaling cascade involving Bcl-2/Bax, cytochrome *c*, and caspase-9/-3 activation. p53, a type of tumor suppressor, can block the cell signaling pathways mediating the tumor progression (Hickman, Moroni et al., 2002). The overexpression of p53 usually induced by DNA damage (Abuetabh, Wu et al., 2022) might be a promising outcome in regulating cellular apoptosis and inhibition of the activity of cancer cells. Thus, p53 over-activation is involved in suppressing cell progression. Indeed, functional p53 serves as a protective marker against tumor proliferation (Carlsson, Vollmer et al., 2022). In our study, we manifested that p53 might trigger mitochondrial apoptosis following oxidative/[Ca^{2+}] stress induced by the nordentatin.

Apoptosis is characterized as an underlying cellular feature arising under different physiologic and pathologic events. In this study, nordentatin, a coumarin-based bioactive compound, was depicted to upregulate the expression level of p53 mRNA. The Bcl-2 family with several pro-apoptotic and anti-apoptotic modulators of apoptosis can be regulated by p53 (Ashkenazi, Fairbrother et al., 2017, Kim, Jung et al., 2017). The Bcl-2 family can protect mitochondrial integrity and deregulation of its balance can result in MMP loss and activation/release of cytochrome *c* which finally causes the activation of caspase-9/-3 as the key executioners of p53-mediated apoptosis (Qian, Shi et al., 2023).

4. Conclusion

Overall, the interaction of nordentatin with AGP as a crucial plasma protein which is capable of binding with different drugs was analyzed by multi-spectroscopic techniques. Molecular docking studies were also done to analysis the interaction of nordentatin with AGP at atomic level. Then, the anticancer activities and mechanism of nordentatin in HCT-116 colorectal cancer cells were assessed. It was revealed that nordentatin potentially interacted with AGP and induced a static quenching mechanism mainly through formation of hydrophobic forces. Nordentatin partially changed the secondary and tertiary structure of AGP. Also, nordentatin induced anticancer effects in HCT-116 colorectal cancer cells through elevation of ROS and [Ca^{2+}], MMP reduction and P53/Bax/Bcl-2/cytochrome *c*/caspase-9/-3 signaling pathway. Thus, nordentatin could be used in the development of anticancer products with good pharmacodynamics and pharmacokinetic properties. Whether nordentatin endows a probable anticancer activity in vivo needs future studies.

Declaration of competing interest

The authors declare that they have no known competing financial interests or personal relationships that could have appeared to influence the work reported in this paper.

Acknowledgments

This study was funded by no Scientific Research Foundation. The authors thank the anonymous reviewers for their valuable advice.

References

Abdelhameed, A.S., Ajmal, M.R., Ponnusamy, K., Subbarao, N., Khan, R.H., 2016. Interaction of the recently approved anticancer drug nintedanib with human acute phase reactant α 1-acid glycoprotein. J. Mol. Struct. 1115, 171–179.

Abdjan, M.I., Aminah, N.S., Siswanto, I., Thant, T.M., Kristanti, A.N., Takaya, Y., 2020. In silico approach: biological prediction of nordentatin derivatives as anticancer agent inhibitors in the cAMP pathway. RSC Adv. 10 (70), 42733–42743.

Abuetabh, Y., Wu, H.H., Chai, C., Al Yousef, H., Persad, S., Sergi, C.M., Leng, R., 2022. DNA damage response revisited: the p53 family and its regulators provide endless cancer therapy opportunities. Exp. Mol. Med. 54 (10), 1658–1669.

Ajmal, M.R., Nusrat, S., Alam, P., Zaidi, N., Badr, G., Mahmoud, M.H., Rajpoot, R.K., Khan, R.H., 2016. Differential mode of interaction of ThioflavinT with native β structural motif in human α 1-acid glycoprotein and cross beta sheet of its amyloid: Biophysical and molecular docking approach. J. Mol. Struct. 1117, 208–217.

Ajmal, M.R., Nusrat, S., Alam, P., Zaidi, N., Khan, M.V., Zaman, M., Shahein, Y.E., Mahmoud, M.H., Badr, G., Khan, R.H., 2017. Interaction of anticancer drug clofarabine with human serum albumin and human α-1 acid glycoprotein. Spectroscopic and molecular docking approach. J. Pharm. Biomed. Anal. 135, 106–115.

AlAjmi, M.F., Rehman, M.T., Khan, R.A., Khan, M.A., Muteeb, G., Khan, M.S., Noman, O. M., Alsalme, A., Hussain, A., 2020. Understanding the interaction between α-1-acid glycoprotein (AGP) and potential Cu/Zn metallo-drugs of benzimidazole derived organic motifs: A multi-spectroscopic and molecular docking study. Spectrochim. Acta Part A: Mol. Biomol. Spectrosc. 225, 117457.

Ashkenazi, A., Fairbrother, W.J., Leverson, J.D., Souers, A.J., 2017. From basic apoptosis discoveries to advanced selective BCL-2 family inhibitors. Nat. Rev. Drug Discov. 16 (4), 273–284.

Boonyarat, C., Boonput, P., Tongloh, N., Kaewamatawong, R., Chaiwiwatrakul, S., Yenjai, C., Waiwut, P., 2022. Nordentatin inhibits neuroblastoma cell proliferation and migration through regulation of GSK-3 pathway. Curr. Issues Mol. Biol. 44 (3), 1062–1074.

Bteich, M., 2019. An overview of albumin and alpha-1-acid glycoprotein main characteristics: highlighting the roles of amino acids in binding kinetics and molecular interactions. Heliyon 5 (11).

Carlsson, M.J., Vollmer, A.S., Demuth, P., Heylmann, D., Reich, D., Quarz, C., Rasenberger, B., Nikolova, T., Hofmann, T.G., Christmann, M., 2022. p53 triggers mitochondrial apoptosis following DNA damage-dependent replication stress by the hepatotoxin methyleugenol. Cell Death Dis. 13 (11), 1009.

Gavrilas, L.I., Cruceriu, D., Mocan, A., Loghin, F., Miere, D., Balacescu, O., 2022. Plant-derived bioactive compounds in colorectal cancer: Insights from combined regimens with conventional chemotherapy to overcome drug-resistance. Biomedicines 10 (8), 1948.

Hickman, E.S., Moroni, M.C., Helin, K., 2002. The role of p53 and pRB in apoptosis and cancer. Curr. Opin. Genet. Dev. 12 (1), 60–66.

Hossain, M.S., Karuniawati, H., Jairoun, A.A., Urbi, Z., Ooi, D.J., John, A., Lim, Y.C., Kibria, K.M.K., Mohiuddin, A.K.M., Ming, L.C., 2022. Colorectal cancer: a review of carcinogenesis, global epidemiology, current challenges, risk factors, preventive and treatment strategies. Cancers 14 (7), 1732.

Huang, J.X., Cooper, M.A., Baker, M.A., Azad, M.A.K., Nation, R.L., Li, J., Velkov, T., 2012. Drug-binding energetics of human α-1-acid glycoprotein assessed by isothermal titration calorimetry and molecular docking simulations. J. Mol. Recognit. 25 (12), 642–656.

Jantakoon, P., Tadtong, S., Puthongking, P., 2012. Neuritogenic and antioxidant activities of nordentatin from Clausena harmandiana. J. Asian Assoc. Schools Pharm. 1, 180–186.

Jantamat, P., Weerapreeyakul, N., Puthongking, P., 2019. Cytotoxicity and apoptosis induction of coumarins and carbazole alkaloids from Clausena harmandiana. Molecules 24 (18), 3385.

Jiang, S.-L., Hu, Z.-Y., Wang, W.-J., Hu, L., Li, L., Kou, S.-B., Shi, J.-H., 2023. Investigation on the binding behavior of human α1-acid glycoprotein with Janus Kinase inhibitor baricitinib: Multi-spectroscopic and molecular simulation methodologies. Int. J. Biol. Macromol., 125096

Jiang, S.-L., Li, L., Hu, L., Kou, S.-B., Shi, J.-H., 2023. Comprehending binding features between ibrutinib and Human Alpha-1 acid glycoprotein: Combined experimental

approaches and theoretical simulations. Spectrochim. Acta Part A: Mol. Biomol. Spectrosc. 285, 121834.
Jiang, S.-L., Li, L., Kou, S.-B., Hu, L., Shi, J.-H., 2023. Insight into intermolecular binding mechanism of apatinib mesylate and human alpha-1-acid glycoprotein: combined multi-spectroscopic approaches with in silico. J. Biomol. Struct. Dyn. 1–12.
Johnson, D.A., Smith, K.D., 2006. The efficacy of certain anti-tuberculosis drugs is affected by binding to α-1-acid glycoprotein. Biomed. Chromatogr. 20 (6–7), 551–560.
Kim, K.Y., Cho, H.J., Yu, S.N., Kim, S.H., Yu, H.S., Park, Y.M., Mirkheshti, N., Kim, S.Y., Song, C.S., Chatterjee, B., 2013. Interplay of reactive oxygen species, intracellular Ca2+ and mitochondrial homeostasis in the apoptosis of prostate cancer cells by deoxypodophyllotoxin. J. Cell. Biochem. 114 (5), 1124–1134.
Kim, E.M., Jung, C.-H., Kim, J., Hwang, S.-G., Park, J.K., Um, H.-D., 2017. The p53/p21 complex regulates cancer cell invasion and apoptosis by targeting Bcl-2 family proteins. Cancer Res. 77 (11), 3092–3100.
Kou, S.-B., Li, L., Zhang, R.-J., Shi, J.-H., Jiang, S.-L., 2023. Elucidation of the interaction mechanism of olmutinib with human α-1 acid glycoprotein: insights from spectroscopic and molecular modeling studies. J. Biomol. Struct. Dyn. 41 (2), 525–537.
Longo, E., Siligardi, G., Hussain, R., 2023. Interaction of blenoxane and congeners bleomycins A2 and B2 with human plasma proteins using circular dichroism spectroscopy. Int. J. Mol. Sci. 24 (17), 13598.
Luo, Z., Boonyaratanakornkit, L., Che, C.-T., Erdelmeier, C.A.J., Fong, H.H.S., Farmworth, N.R., 1986. Biologically active coumarins from Enkleia siamensis. J. Nat. Prod. 49 (6), 1161–1162.
Luo, Z., Lei, H., Sun, Y., Liu, X., Su, D.-F., 2015. Orosomucoid, an acute response protein with multiple modulating activities. J. Physiol. Biochem. 71, 329–340.
Maruyama, T., Otagiri, M., Schulman, S.G., 1990. Binding characteristics of coumarin anticoagulants to human α1-acid glycoprotein and human serum albumin. Int. J. Pharm. 59 (2), 137–143.
Owczarzy, A., Rogóż, W., Kulig, K., Pożycka, J., Zięba, A., Maciążek-Jurczyk, M., 2023. Spectroscopic studies of quinobenzothiazine derivative in terms of the in vitro interaction with selected human plasma proteins: Part 2. Molecules 28 (2), 698.
Qian, Y., Shi, C., Cheng, C., Liao, D., Liu, J., Chen, G.-T., 2023. Ginger polysaccharide UGP1 suppressed human colon cancer growth via p53, Bax/Bcl-2, caspase-3 pathways and immunomodulation. Food Sci. Human Wellness 12 (2), 467–476.
Schmidt, S., Gonzalez, D., Derendorf, H., 2010. Significance of protein binding in pharmacokinetics and pharmacodynamics. J. Pharm. Sci. 99 (3), 1107–1122.
Schmidt, S., Zehe, M., Holzgrabe, U., 2023. Characterization of binding properties of ephedrine derivatives to human alpha-1-acid glycoprotein. Eur. J. Pharm. Sci. 181, 106333.
Siddiqui, A. J., S. Jahan, R. Singh, J. Saxena, S. A. Ashraf, A. Khan, R. K. Choudhary, S. Balakrishnan, R. Badraoui and F. Bardakci (2022). "Plants in anticancer drug discovery: from molecular mechanism to chemoprevention." BioMed Research International **2022**.
Tsai, C.-C., Li, Y.-S., Lin, P.-P., 2017. Inonotus obliquus extract induces apoptosis in the human colorectal carcinoma's HCT-116 cell line. Biomed. Pharmacother. 96, 1119–1126.
Ullah, R., Rehman, N.U., Jamshidi-Adegani, F., Bari, A., 2022. Medicinal plants and marine-derived natural products as cancer chemopreventive agents. Front. Pharmacol. 13, 900275.
Wang, B.-L., Kou, S.-B., Lin, Z.-Y., Shi, J.-H., 2020. Insight into the binding behavior of ceritinib on human α-1 acid glycoprotein: Multi-spectroscopic and molecular modeling approaches. Spectrochim. Acta Part A: Mol. Biomol. Spectrosc. 232, 118160.
Wang, B.-L., Kou, S.-B., Lin, Z.-Y., Shi, J.-H., Liu, Y.-X., 2020. Insights on the interaction mechanism of brigatinib to human α-1-acid glycoprotein: Experimental and computational approaches. Int. J. Biol. Macromol. 157, 340–349.
Wang, X., Sun, J., Ma, L., Nie, Z., Sai, H., Cheng, J., Duan, J., 2023. Characterization of the interactions between minocycline hydrochloride and trypsin with spectroscopic and molecular docking technology. Molecules 28 (6), 2656.
Yeggoni, D.P., Rachamallu, A., Kallubai, M., Subramanyam, R., 2015. Cytotoxicity and comparative binding mechanism of piperine with human serum albumin and α-1-acid glycoprotein. J. Biomol. Struct. Dyn. 33 (6), 1336–1351.
Yeggoni, D.P., Meti, M., Subramanyam, R., 2023. Chebulinic and chebulagic acid binding with serum proteins: biophysical and molecular docking approach. J. Biomol. Struct. Dyn. 41 (9), 4024–4039.
Yu, Y.-H., Wang, L., Zhang, Q., Zhang, X.-N., Zhao, X.-H., 2022. Activities of the soluble and non-digestible longan (Dimocarpus longan Lour.) polysaccharides against HCT-116 cells as affected by a chemical selenylation. Curr. Res. Food Sci. 5, 1071–1083.
Zhou, Y., Jing, S., Liu, S., Shen, X., Cai, L., Zhu, C., Zhao, Y., Pang, M., 2022. Double-activation of mitochondrial permeability transition pore opening via calcium overload and reactive oxygen species for cancer therapy. J. Nanobiotechnol. 20 (1), 1–14.
Zsila, F., Mády, G., 2008. Biliverdin is the endogenous ligand of human serum α1-acid glycoprotein. Biochem. Biophys. Res. Commun. 372 (3), 503–507.
Zsila, F., Bősze, S., Beke-Somfai, T., 2020. Interaction of antitubercular drug candidates with α1-acid glycoprotein produced in pulmonary granulomas. Int. J. Biol. Macromol. 147, 1318–1327.